ISBN: 978-3-95450-204-2 ISSN: 2673-5350 doi:10.18429/JACoW-IBIC2019-TUBO01

SCREENS FOR HIGH PRECISION MEASUREMENTS*

B. Walasek-Höhne†, P. Forck, GSI, Darmstadt, Germany
K. Höhne, FAIR, Darmstadt, Germany
G. Kube, DESY, Hamburg, Germany
R. Ischebeck, PSI, Villingen, Switzerland

Abstract

Scintillation screens made of various inorganic materials are widely used for transverse beam profile diagnostics at all kinds of accelerators. The monitor principle is based on the particles' energy loss and its conversion to visible light. The resulting light spot is a direct image of the two-dimensional beam distribution. For large beam sizes standard optical techniques can be applied, while for small beam sizes dedicated optical arrangements have to be used to prevent for image deformations. In the modern linac based light sources scintillator usage serves as an alternative way to overcome limitations related to coherent OTR emission. Radiation damages and intensity based saturation effects, in dependence of the screen material, have to be modelled. In this proceeding, an introduction to the scintillation mechanism in inorganic materials will be given including practical demands and limitations. An overview on actual applications at hadron and electron accelerators will be discussed as summary of the Joint ARIES-ADA Workshop on 'Scintillation Screens and Optical Technology for transverse Profile Measurements' held in Krakow, Poland [1].

INTRODUCTION / APPLICATION

Scintillators are used since the early days of nuclear physics. In hadron and electron accelerators they are used for transverse beam profile measurements and in high energy physics for particle detection and tracking.

Profile measurements are important for controlling the spatial distribution of the particle beam, as well as the matching of different sections of the accelerator. The performance and safe operation of particle accelerators is closely connected to the matching of the transverse beam distribution. Scintillating screens are a direct, but intercepting, method to observe transverse beam profiles. A measurement can hardly be more intuitive than to see a beam spot right in the centre of a scintillating screen. One typical realisation is shown in Fig. 1. For this reason many investigations have been done over years to achieve precise monitoring of the particle distribution along accelerator chains with scintillating screens.

Over the last century a large number of organic and inorganic scintillators in all physical states were discovered. In diagnostics inorganic solid state scintillators, such as crystals, powder crystals or ceramics, are mainly used. The response of scintillating materials depends on beam parameters such as energy, intensity, ion species and time structure. Therefore, scintillating materials have to be tailored with respect to specific application demands required at accelerator facilities. Due to the direct beam interaction, many investigations described in this paper were performed for particle fluxes much higher than for typical scintillator applications in medical imaging or high energy physics. Table 1 gives a simplified overview of scintillator usage in beam diagnostics at ion and electron accelerators, and typical high-energy physics applications, e.g. PANDA detector at FAIR.

Precise measurements of the size, profile and position of a particle beam striking a scintillating screen requires a carefully designed optical system to transfer the scintillation light to the camera, so the true particle distribution can be reconstructed. Aim is to capture a clean, sharply focused image of the scintillation plane, free of distortion, optical aberrations, non-linearity, or optical backgrounds.

SCINTILLATION

A beam of ionizing radiation passing through a scintillator generates electronic exicitations. The relaxation of electronic excitations involves complex mechanisms which can be described using a scheme of the electronic band structure of the crystalline scintillator. As proposed by Vasil'ev [2], the general time-dependent scheme of scintillation can be described in five main stages. The first stage starts with the production of primary excitations (deep core holes and hot electrons) by interaction of ionizing particles with the material. In a very short time (10^{-16}-10^{-14} s) a large number of secondary electronic excitations is produced by inelastic electron–electron (e–e) scattering and Auger processes with creation of electrons in the conduction band and holes in core and valance bands. This multiplication is stopped when the energy of electrons and holes becomes lower than the threshold of e–e scattering and Auger relaxation. The second stage deals with the thermalization of electrons and holes with the production of e.g. phonons. In the third stage localization of the excitations through their interaction with stable defects and material impurities can take place. It may occur together with formation of self-trapped excitons (trapping due to lattice relaxation, not attributed to crystalline defects or impurities) and holes in the crystal lattice, the capture of electrons and holes by traps, etc. As a result, these centers have localized states in the band gap. The two last steps are related with migration of relaxed excitations and radiative or/and nonradiative recombination of localized excitations (fourth stage). The localization of excitations is sometimes accompanied by a displacement of atoms (defect creation,

* This project has received funding from the European Union's Horizon 2020 programme under Grant Agreement No 730871
† b.walasek@gsi.de

ISBN: 978-3-95450-204-2 ISSN: 2673-5350 doi:10.18429/JACoW-IBIC2019-TUBO01

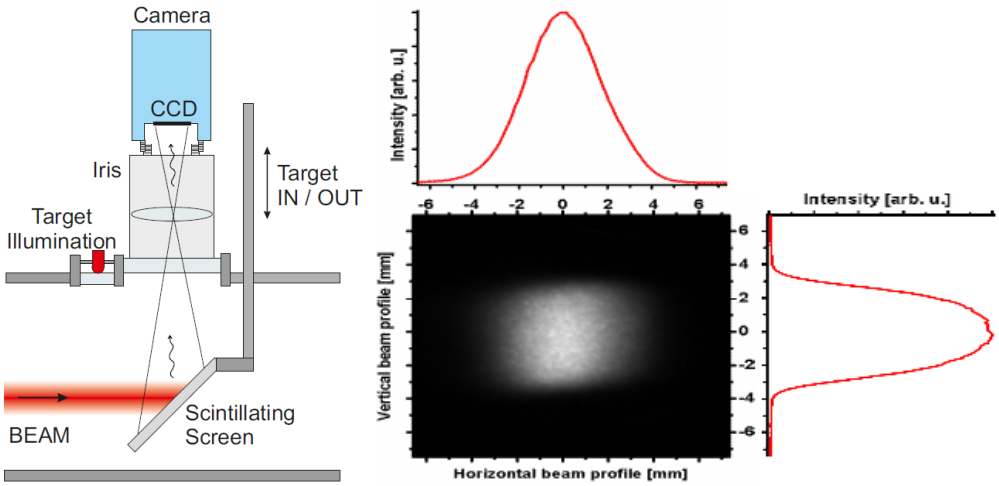

Figure 1: Typical setup of a scintillating screen in beam diagnostics application.

Table 1: Simplified Overview of Scintillator Usage in Beam Diagnostics and High Energy Physics

	Ion Diagnostic	**Electron Diagnostic**	**High Energy Physics**
Application	Primary beam on screen, transverse beam profile	Primary beam on screen, transverse beam profile	Detection of secondary particles, tracking, timing
Particle energy	1 keV/u – 100 GeV/u	100 keV – 10 GeV	up to 10 GeV
Spot size	1 mm – 1 cm	1 µm – 1 mm	1 cm – 100 cm
Particle rate	very high	very high	low
Dose rate	very high	high	low
Energy deposition	very large	medium	low
Saturation	expected	possible	none
Modification	expected	possible	low

photo-stimulated desorption). The fifth stage describes the luminescence of emitting centers excited by the final electronic excitations (correlated electron-hole pairs, excitons, separated electrons, holes, etc.) through sequential capture of charge carriers or various energy transfer processes.

The scintillation mechanism as described in detail above is a complicated process, variable for different materials and influenced by several factors like:

- Temperature: thermal quenching is related to electron-phonon interactions and may lead to radiation-less processes. In the typical case, with rising temperature the light yield of the material and the decay time decreases.
- Concentration of luminescence centres: the interaction between luminescence centres increases with their density in the material. At high densities, energy migration through non-radiative energy transfer might take place.
- Impurities in material: killer ions can compete with active ions and limit the scintillation efficiency.
- High energy deposition: relaxation of electronic excitation might lead to the formation of nanometric scale regions containing several electronic excitations separated by a short distance (local density-induced quenching).

In beam diagnostic applications, the energy conversion from incoming ions or electrons is even a more complicated process. Due to high energy deposition in the scintillating material several non-proportional effects as described in [3–5] have to be considered. A simple analytical model was proposed by Michaelian et al. [6] for the ion-induced scintillation response of detector materials. With this model predictions over a wide range of incident ion species and energies are obtained. The fundamental variables characterizing the luminescent response of the ion-target material interaction are found to be the velocity v and effective charge z_{eff} of the incident ion and the effective charge Z_{eff}, mass A, mass density ρ and the quenching energy density ρq of the material. Two more material specific constants are required characterizing the energy to light conversion process for the impurity activated inorganic and the organic materials.

Inorganic scintillators are widely used for the detection of ionizing radiation. In the past decades significant progress in the discovery of many new materials and description of the basic physical processes has been made. Reviewing many beam diagnostic applications [7] among the most important properties of a good scintillator are:

- sufficient efficiency in energy conversion into light,
- large dynamic range and good linearity between incident particle flux and light yield,
- emission spectra matched to the spectral response of the photon detector (e.g. standard CCD camera),
- no absorption of emitted light inside the bulk material to prevent artificial broadening by stray light,

ISBN: 978-3-95450-204-2 ISSN: 2673-5350 doi:10.18429/JACoW-IBIC2019-TUB001

- short decay time for observations of time dependent beam size variations and reduction of saturation effects,
- good mechanical and thermal stability,
- high radiation hardness to prevent material damages.

The most widely used materials for manufacturing of scintillating screens in beam diagnostics are the following:

- Crystals e.g. YAG:Ce ($Y_3Al_5O_{12}$:Ce), BGO ($Bi_4Ge_3O_{12}$), LYSO ($Lu_{1.8}Y_{0.2}SiO_5$:Ce) or CWO ($CdWO_4$). Scintillators made of single crystals have been proposed for beam diagnostics long time ago. However, their usage is limited by the demand of screens in big sizes. Crystals give good light yield, but show degradation effects under high current beam irradiations.
- Powder crystals e.g. P43 (Gd_2O_2S:Tb), P46 ($Y_3Al_5O_{12}$:Ce) or P47 ($Y_2Si_5O_5$:Tb). These screens are manufactured by deposition of luminescence powder on a glass or metal base. They can be designed in flexible sizes and shapes, but easily damaged due to mechanical stress. The sensitivity of such phosphors is high and they are characterized by good linearity. The emitted light is reflected many times in the material before the exit from the grain of the powder. This leads to scintillation of the whole grain, whereas the resolution is limited by the average grain size.
- Ceramics e.g. ZrO_2:Al, ZrO_2:Mg, ZrO_2:Y, Al_2O_3, ruby ceramics (Al_2O_3:Cr), AlN or BN. Ceramics screens are usually made by sintering of powder. These materials have moderate light yield, but their radiation hardness and thermo-mechanical properties are better.

SCREENS FOR ION BEAMS

The energy loss of particle beams in material is described by the Bethe-Bloch equation

$$-\frac{dE}{dx} = \frac{4\pi n z^2}{m_e c^2 \beta^2}\left(\frac{e^2}{4\pi\varepsilon_0}\right)^2\left[ln\left(\frac{2m_e c^2\beta^2}{I(1-\beta^2)}\right) - \beta^2\right]. \quad (1)$$

The energy loss depends on the charge z and the velocity $\beta = v/c$ of the incident particle and the electron density n and mean excitation potential I of the target material. The electron density is given by the atomic number Z, the density ρ and the inverse of the mass: $n = \frac{Z\cdot\rho}{A\cdot u}$. The mean excitation potential is proportional to the atomic number. An approximation given by Bloch is $I = (10\text{ eV})\cdot Z$ [8]. Figure 2 shows the energy loss of a ^{63}Cu beam in an Al_2O_3 scintillator. Even for low energy ion beams with energies of a few MeV/u the nuclear stopping is negligible w.r.t to the electronic stopping. The maximum electronic stopping is at approximately 3 MeV/u.

The energy loss of high energy ion beams with kinetic energy $E_{kin} > 100$ MeV/u in material is low (cf. Fig. 2 green shaded area). The particle range is larger than the screen thickness and they deposit less energy in the material, leading to less material heating around the ion track; this is confirmed by comparing the radiation damage as a function of fluence for ions in the range of MeV/u to the significantly lower damage of ions in the range of several 100 MeV/u.

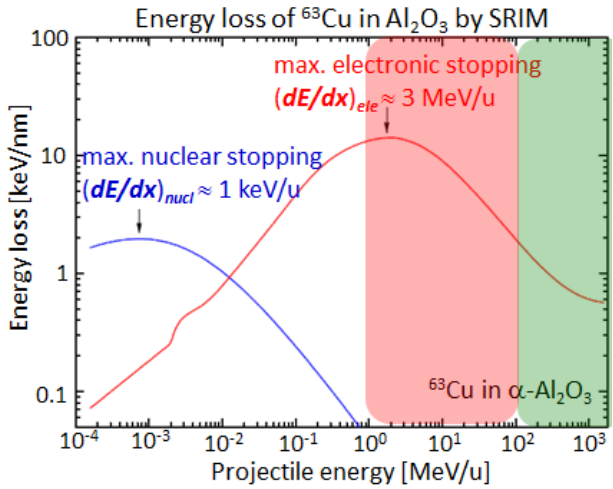

Figure 2: Energy loss of ^{63}Cu in Al_2O_3 by electronic (red line) and nuclear stopping (blue line). The red area indicates low energy ion beams, the green area high energy ion beams.

During several investigations, the several inorganic scintillators showed a great stability as reported in [9]. Non-linear characteristics, e.g. due to quenching during irradiation at high beam intensities, were not observed. The light yield S showed a tendency to decrease with increasing calculated electronic energy loss dE/dx. The characteristics of the calculated beam profiles as well as the recorded emission spectra did not change significantly. Neither structural variations nor material defects, induced by the ion irradiation, were proven with analytical methods like UV/VIS transmission spectroscopy, X-Ray diffraction and Raman fluorescence spectroscopy and the given ion fluencies.

In case of low energy ion beams several degradation effects have been observed. E.g. over the time standard used Chromox screen was fading [10], Al_2O_3 light yield decreased and ZrO_2 surface was coloured [11]. Low energy ion beams 1 MeV/u $< E_{kin} <$ 100 MeV/u have a large energy loss in material (cf. Fig. 2 red shaded area) which results in large damage in the scintillator.

To investigate the radiation damage processes in detail, the un-doped Al_2O_3 was investigated with different ions in the energy range 0.5 to 5.9 MeV/u within a broad range of fluences up to some 10^{14} cm^{-2} at GSI [12]. The ion induced displacements at some MeV/u ions are not attributed to nuclear stopping. The damage is caused by the large electronic stopping power (close to the maximum of Bethe-Bloch equation), which heats the material around the ion track and leads to amorphisation and therefore for an increasing density of colour centres. Al_2O_3 is an intrinsic scintillator, the luminescence is originated from different colour centres with maxima in the wavelength range of λ from 322 to 413 nm. After radiation with a low fluence like 10^{12} cm^{-2}, the surface of the ceramic discoloured at the beam spot; the additional colour centres are created. The light yield during irradiation

ISBN: 978-3-95450-204-2 ISSN: 2673-5350 doi:10.18429/JACoW-IBIC2019-TUBO01

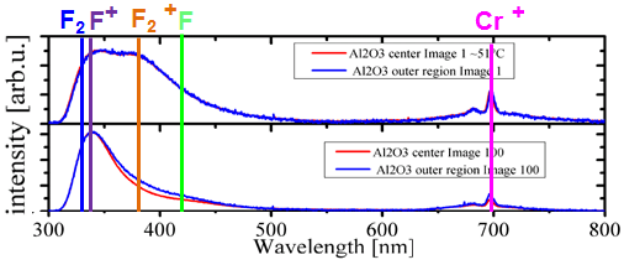

Figure 3: Light emission spectrum of Al_2O_3 after first pulse (top) and after 100 pulses (bottom). Beam parameters: Ca^{10+}, 4.8 MeV/u, $5 \cdot 10^{10}$ ppp in 3.3 ms. Lines indicate the emission lines of the color centers [13].

decreases, but the rate depends significantly on the colour centre type, the F^+ centre (maximum at $\lambda = 326$ nm) is much more radiation hard than other centres (cf. Fig. 3) [12].

The decreasing light yield S as a function of fluence Φ can be described by the so called Birks model which uses macroscopic quantities damage cross section σ_D and quenching ratio K

$$S(\Phi) = S_0 \cdot \frac{1}{1 + K - \exp(-\sigma_D \Phi)}. \qquad (2)$$

The light yield caused by radiation damage decreases initially proportional to $S_0/(1 + K\sigma_D\Phi)$, but levels off to a constant level $S_0/(1 + K)$ for large fluences. In Fig. 4 experimental results for an Al_2O_3 screen irradiated with a low energy Cu beam are plotted. The Birks fit shows good agreement with the observed data [12]. This behaviour is explained by an increasing probability that a projectile induced displaced atom is stopped in a corresponding location cancelling the damage effects [13]. The Birks model was applied to other ceramic scintillators showing the same general behaviour and turn out to be also good fit for measurements decay of Al_2O_3:Cr at the Spallation Neutron Source reported in [14].

The investigations reported in [12] show, that Al_2O_3 is most radiation hard, i.e. has lowest damage cross section and low quenching ratio. Analysis of the optical absorption measurements show that the degradation of the scintillation yield can be decelerated significantly or even stopped at elevated temperatures (575 to 773 K), but decrease of the yield by the thermal quenching must be considered. Heating of the target represents an effective tool to increase usable lifetime of the scintillating screen. After thermal annealing of 1 h at 1073 K Al_2O_3 regains its original properties [12]. Thermal annealing would enable precise profile and emittance measurements even for high beam currents at low energies.

SCREENS FOR ELECTRON BEAMS

While ion beam size is in the range from mm to cm the electron beam size ranges from below 1 mm down to some µm. The standard method determine the transverse beam profile in electron machines uses the optical transition radiation (OTR). OTR is a classical electro-dynamic process, as produced by a charged particle crossing the boundary

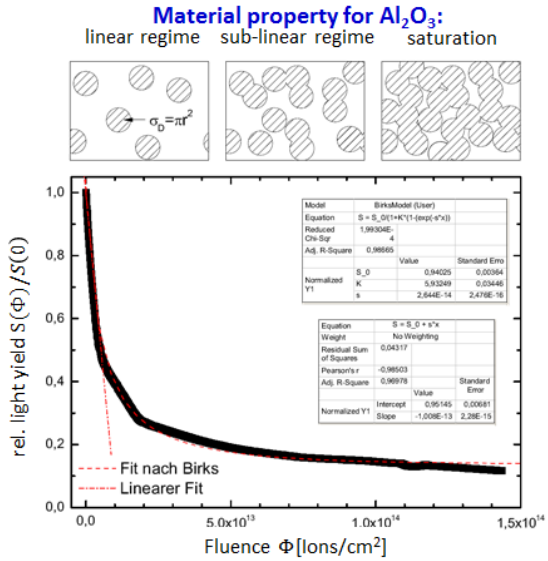

Figure 4: Relative light yield $S(\Phi)/S_0$ of Al_2O_3 irradiated with a 0.5 MeV/u Cu beam. Measured data (black), Birks fit with $\sigma_D = 2.64 \cdot 10^{-14}$ cm^2 and $K = 5.93$ (red dashed) [12].

between two media of different dielectric constants. Scintillating screens are commonly used for transverse profile measurements at low energy electron machines where the intensity of OTR is rather low. Linac based FELs produce ultra-short bunches with low longitudinal emittance (energy spread). The high peak current and microbunching instability conspire to generate Coherent Optical Transition Radiation (COTR) at the surface of all profile monitor screen materials. The COTR is both unstable and many orders of magnitude brighter. Standard beam profile measurements based on OTR may be hampered by coherence effects. By using a scintillation screen in combination with a fast gated CCD camera, coherence effects can be suppressed, as OTR is created in an instantaneous process while scintillation light has a certain decay time.

Comparisons between YAG screen, OTR and wire scanner showed good agreement between all three methods down to 60 µm. Even the detailed beam structure during one bunch was observed with the $Y_3Al_5O_{12}$:Ce screen [15, 16]. Investigations of several scintillators were done with a 855 MeV cw electron beam of beam size 25 µm with currents between 10 pA and 50 nA [17]. The first observation is the material dependency of the observed beam size. The beam size measured with different 0.3 mm thick scintillating screens varies between 25.5 µm (CRY019) and 34.2 µm ($Y_3Al_5O_{12}$:Ce). The beam size measured with scintillating screens is always larger than measured with OTR. In principle, this observation is confirmed by [18], although the results for some materials deviate quantitatively. This might be due to different scintillator thicknesses, material treatment (ITO coating), or beam parameters. The second observation is a strong dependency on the optical setup, which is independent of the screen material [17, 18] (cf. section Optical Setup for de-

ISBN: 978-3-95450-204-2 ISSN: 2673-5350 doi:10.18429/JACoW-IBIC2019-TUB001

tails). The third observation is a dependency of the observed beam size on the thickness of the scintillator [17, 19].

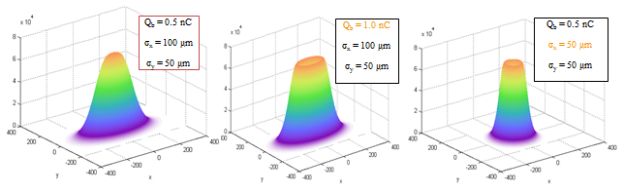

Figure 5: Calculated beam profiles using the simple model to describe smoke ring shaped beam distributions as observed at the European XFEL. A Gaussian profile (left) results in smoke ring shaped beam profiles by increasing the bunch charge (middle) or reducing the beam size (left) [20].

It was decided for the European XFEL to measure transverse beam profiles based on scintillating screen monitors using LYSO:Ce. While it is possible to resolve beam sizes down to a few micrometers with this scintillator, the experience during the XFEL commissioning showed that the measured emittance values were significantly larger than the expected ones. In addition, beam profiles measured at bunch charges of a few hundred pC showed a 'smoke ring' structure. While COTR emission and beam dynamical influence can be excluded, it is assumed that the profile distortions are caused by effects from the scintillator material. A simple model was developed which takes into account quenching effects of excitonic carriers inside a scintillator in a heuristic way [20]. Based on this model, the observed beam profiles can be understood qualitatively as a non-linear effect of the scintillator (cf. Fig. 5). For LYSO scintillators, the high density thresholds were in the order of 1 nC beams into 100 µm. Currently, different screens to reduce this effect are under investigation, both theoretically and experimentally. Theoretically, the quest is focused on Gadolinium-based scintillators (where charge carriers rapidly transfer their energy to the excited state of Gadolinium), or YAP (where high mobility of excitation carriers reduce the quenching probability). The first tests with YAP and YAG:Ce showed better results than with LYSO [20].

Another non-linear effect of the scintillator has been reported in [21]. There is an overestimation of the beam size due to saturation. The saturation modifies the original Gaussian distribution with a reduction factor. Measurements with LYSO, YAG:Ce and BGO indicate that saturation occurs above 1 nC/mm^2.

With boron nitride nano tubes a new scintillator material was presented during ARIES-ADA Workshop, having the advantage that it is very radiation resistant and suitable for high power beam applications. The first experiments with this material were performed for beam energies from 300 keV up to 11 GeV and first results can be found in [22].

OPTICAL SETUP

The measured beam size does not depend on the scintillator material only. Using scintillating screens for high precision measurements requires carefully designed optical setups. One typical realisation is shown in Fig. 1 and Fig. 6 (a). The scintillating screen is inserted into the beam under an angle of 45°. Through a viewport, located at 90° with respect to the beam, a camera observes the screen. Several others commonly used layouts to image the scintillation light onto detector are applied in beam instrumentation as shown in Fig. 6 (b)–(d). Direct detection of the light Fig. 6 (b) may easily lead to radiation damage of the detector and problems with implementation into ultrahigh vacuum systems. In setups with off-axis light detection the horizontal resolution is limited to the scintillator thickness because points points along the primary beam axis are imaged to different locations on the detector.

Usage of in-vacuum mirrors as shown in Fig. 6 (c) can improve the resolution, smaller than thickness of the screen, however the radiation damage of the mirror which can interact with primary beam can lead to loss of reflectivity. The field of view is limited by the depth of field of the optical system. Applying the Scheimpflug principle Fig. 6 (d), in which object (scintillator), lens plane and detector (image) plane intersect in the single line, the object plane is completely in the sharp focus. This improves the field of view, but the limitation due to the scintillator thickness remains.

In general, the observation of a scintillator of finite thickness d and index of refraction n depends on the angles of the incident particle α and the observation β. Figure 7 sketches the geometry. A particle beam generates a scintillating chan-

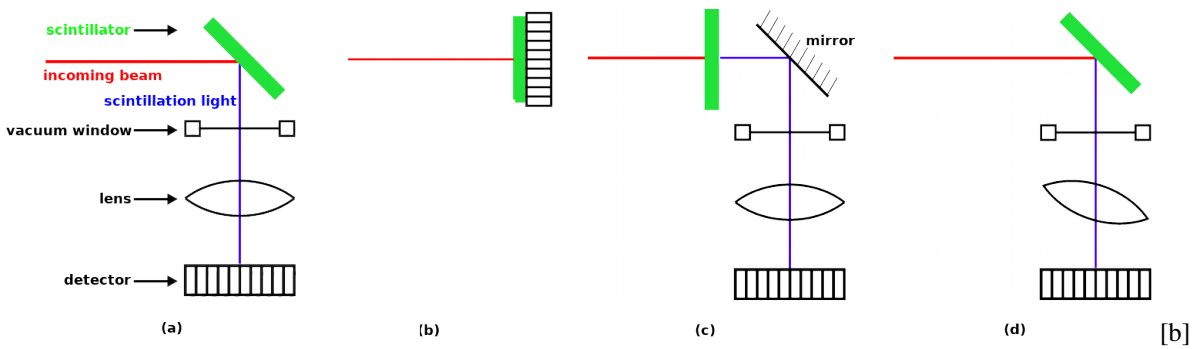

Figure 6: Typical optical setups of scintillating screens in beam diagnostics. (a) with tilted screen by 45°, (b) in beam detector, (c) with mirror, and (d) with Scheimpflug geometry.

ISBN: 978-3-95450-204-2 ISSN: 2673-5350 doi:10.18429/JACoW-IBIC2019-TUBO01

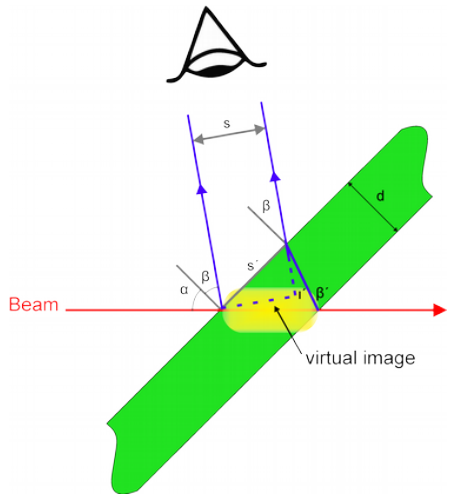

Figure 7: Observation geometry of a scintillation screen. The beam hits the screen with an angle α and the scintillation light is observed at an angle β. Both angles are w.r.t. the normal of the screen.

nel along its axis through the entire depth of the screen. The transverse size of this channel depends on the properties of the scintillator. E.g. powdered scintillators show significant broadening due to light scattering within the screen volume. One can consider, a beam with zero transverse size passes the scintillator undeflected and emission of the scintillation light is isotropic. The beam generates a scintillating channel of a length $(d/\cos\alpha)$. The observed transverse size s of the virtual image is affected by the refraction of the scintillation light at the boundary between scintillator and vacuum. Snell-Descartes law of refraction and the observation geometry lead to

$$s = d\cos\beta\sqrt{\frac{1}{1-\frac{\sin^2\beta}{n^2}}+\frac{1}{\cos^2\alpha}-\frac{2\cos\left(\sin^{-1}\frac{\sin\beta}{n}+\alpha\right)}{\sqrt{1-\frac{\sin^2\beta}{n^2}}\cos\alpha}}. \quad (3)$$

The scintillating channel can be imaged onto a single point on the detector, i.e. the apparent size is zero ($s = 0$), when the viewing angle is

$$\beta_{\text{ideal}} = -\sin^{-1}(n\sin\alpha) \quad (4)$$

For $\alpha = 0$, the ideal observation angle is $\beta = 0$, corresponding to the geometry shown in Fig. 6 (b). Such a setup is often used for observation of low energy electron or ion beams.

This angle dependency has been verified by experiments. In [18] a laser beam ($\lambda = 410$ nm) hits a $Y_3Al_5O_{12}$:Ce screen of thickness $d = 500\,\mu$m at $\alpha = 24°$. The results are shown in Fig. 8. The experimental data (circles) confirm the strong dependency of the observed beam size on the observation angle. Also experiments with 855 MeV electron beams on 300 µm $Bi_4Ge_3O_{12}$ screens show the strong dependency of the observation angle [17].

In addition to the observation geometry, the resolution at the image plane can be influenced by diffraction at any restrictive apertures, around obstructions (dust), or aberrations due to lens imperfections or refractive index variations in the optical system. A Schwarzschild objective, consisting of two concentric spherical mirrors, allows a large numerical aperture and the elimination of spherical and chromatic aberrations. The use of Schwarzschild objectives in scintillation screens in electron machines has been reported in [23, 24].

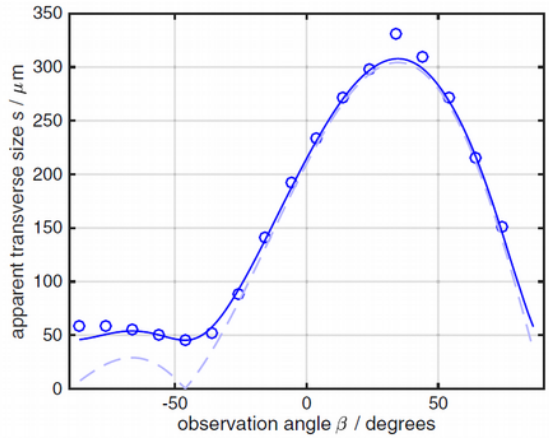

Figure 8: Dependency of the observed beam size s on the observation angle β. Laser beam ($\lambda = 410$ nm) at $\alpha = 24°$ on a $Y_3Al_5O_{12}$:Ce screen of thickness $d = 500\,\mu$m [18].

An important parameter to determine is the point spread function (PSF) of the optical setup. The PSF is the optical response of the system to a single point of light. In the case of a beam profile measurement each charged particle gives a single point of light in the object plane. The measurement and/or calculation of the PSF allows a deconvolution of the image to enhance the resolution.

One example for the strength of this method is given in [24]. The scintillator properties and the optical setup was simulated with the optical ray-tracing program ZEMAX©. The resulting 2-dim. SPF was convoluted with a 2-dim. Gaussian distribution representing the electron beam profile. A vertical cut through the maximum was compared with an vertical cut through the maximum of the measured data from a 200 µm thick LYSO scintillator. By using this technique it was possible to resolve a vertical beam size of 1.44 µm with a scintillating screen.

Today's possibilities of data acquisition by digital cameras and the post-processing tools give a lot of possibilities to increase the performance of scintillator based beam profile measurements.

CONCLUSION

In general, scintillating screens are a good choice for precise beam profile measurements in ion and electron machines. The measured beam profile depends on the observed beam, the screen material and the optical setup. Therefore, the higher the demands on the measurement the more care has to be taken for proper choice of scintillator and optical setup.

ISBN: 978-3-95450-204-2 ISSN: 2673-5350 doi:10.18429/JACoW-IBIC2019-TUBO01

ACKNOWLEDGEMENT

It is a pleasure to acknowledge many stimulating and informative discussions with the participants of the Joint ARIES-ADA Workshop on 'Scintillation Screens and Optical Technology for transverse Profile Measurements' held in April 2019 in Krakow. In particular we would like to thank Enrico Bravin, Ubaldo Iriso, Rhodri Jones, Thibaut Lefevre, Alicja Surowiec and Adriana Wawrzyniak.

REFERENCES

[1] ARIES-ADA Topical Workshop on *Scintillation Screens and Optical Technology for Transverse Profile Measurements*, Krakow, Poland, 2019. https://indico.cern.ch/event/765975/

[2] A. N. Vasil'ev, "A Relaxation of hot electronic excitations in scintillators: account for scattering, track effects, complicated electronic structure", in *Proc. SCINT'99*, (ed.) V. V. Mikhailin, Moscow State Univ., Moscow, 2000, pp. 43–52.

[3] W. W. Moses *et al.*, "Scintillator Non-Proportionality: Present Understanding and Future Challenges", *IEEE Trans. Nucl. Sci.*, vol. 55, pp. 1049–1053, 2008. doi:10.1109/TNS.2008.922802

[4] Qi Li *et al.*, "A transport-based model of material trends in non-proportionality of scintillators", *J. Appl. Phys.*, vol. 109, p. 23716, 2011. doi:10.1063/1.3600070

[5] A. N. Vasil'ev, "From Luminescence Non-Linearity to Scintillation Non-Proportionality", *IEEE Transactions on Nuclear Science*, vol. 55, pp. 1054–1061, 2008. doi:10.1109/TNS.2007.914367

[6] K. Michaelian *et al.*, "Scintillation response of nuclear particle detectors", *Nucl. Instrum. Methods Phys. Res., Sect. A*, vol. 356, pp. 297-303, 1995. doi:10.1016/0168-9002(94)01252-0

[7] P. Forck, "Lecture notes on Beam Instrumentation and Diagnostics", Joint Universities Accelerator School, JUAS 2010. https://www-bd.gsi.de/conf/juas/juas_script.pdf

[8] F. Bloch, "Zur Bremsung rasch bewegter Teilchen beim Durchgang durch Materie", *Annalen der Physik*, vol 408, pp. 285–320, 1933. WILEY-VCH Verlag GmbH, Weinheim, Germany. doi:10.1002/andp.19334080303

[9] A. Lieberwirth *et al.*, "Response from inorganic scintillation screens induced by high energetic ions", *Nucl. Instrum. Methods Phys. Res., Sect. B*, vol. 365, pp. 533–539, 2015. doi:10.1016/j.nimb.2015.07.111

[10] C. B. Bal *et al.*, "Scintillating Screens Study for LEIR/LHC Heavy Ion Beams", in *Proc. DIPAC'05*, Lyon, France, Jun. 2005, paper POM013, pp. 57–59.

[11] E. Bravin, "Scintillating screens use at CERN", Scintillating Screen Applications in beam diagnostics Workshop Darmstadt, 2011. https://www-bd.gsi.de/ssabd/

[12] S. Lederer *et al.*, "Thermal annealing behavior of α-Al_2O_3 scintillation screens", *Nucl. Instrum. Methods Phys. Res., Sect. B*, vol. 365, pp. 548–552, 2015. doi:10.1016/j.nimb.2015.08.024

[13] P. Forck, "Radiation hardness investigations of Al_2O_3 for MeV/u ions at GSI", ARIES-ADA Topical Workshop, Krakow, Poland, 2019. https://indico.cern.ch/event/765975/

[14] W. Blokland, "Screens from the SNS-Target", ARIES-ADA Topical Workshop, 2019. https://indico.cern.ch/event/765975/

[15] S. Rimjaem *et al.*, "Comparison of Different Radiators used to Measure the Transverse Characteristics of Low Energy Electron Beams at PITZ", in *Proc. DIPAC'11*, Hamburg, Germany, May 2011, paper TUPD54, pp. 428–430.

[16] R. Ischebeck, "Scintillators for SwissFEL", Scintillating Screen Applications in beam diagnostics Workshop Darmstadt, 2011. https://www-bd.gsi.de/ssabd/

[17] G. Kube *et al.*, "Inorganic Scintillators for Particle Beam Profile Diagnostics of Highly Brilliant and Highly Energetic Electron Beams", in *Proc. IPAC'12*, New Orleans, LA, USA, May 2012, paper WEOAA02, pp. 2119–2121.

[18] R. Ischebeck *et al.*, "Transverse profile imager for ultra-bright electron beams", *Phys. Rev. Spec. Top. Accel Beams*, vol. 18, p. 082802, 2015. doi:10.1103/PhysRevSTAB.18.082802

[19] G. Kube, C. Behrens, and W. Lauth, "Resolution Studies of Inorganic Scintillation Screens for High Energy and High Brilliance Electron Beams", in *Proc. IPAC'10*, Kyoto, Japan, May 2010, paper MOPD088, pp. 906–908.

[20] G. Kube, S. Liu, A.I. Novokshonov, and M. Scholz, "A Simple Model to Describe Smoke Ring Shaped Beam Profile Measurements With Scintillating Screens at the European XFEL", in *Proc. IBIC'18*, Shanghai, China, Sep. 2018, pp. 366–370. doi:10.18429/JACoW-IBIC2018-WEOC03

[21] F. Miyahara *et al.*, "Response of Scintillating Screens to High Charge Density Electron Beam", in *Proc. IPAC'17*, Copenhagen, Denmark, May 2017, pp. 268–270. doi:10.18429/JACoW-IPAC2017-MOPAB067

[22] K. Jordan, "Jefferson Lab Scintillating Screens", ARIES-ADA Topical Workshop, Krakow, Poland, 2019. https://indico.cern.ch/event/765975/

[23] L. Bobb, "Performance of a Reflective Microscope Objective and Thin Scintillator in an X-ray Pinhole Camera", ARIES-ADA Topical Workshop, Krakow, Poland, 2019. https://indico.cern.ch/event/765975/

[24] G. Kube *et al.*, "Transverse Beam Profile Imaging of Few-Micrometer Beam Sizes Based on a Scintillator Screen", in *Proc. IBIC'15*, Melbourne, Australia, Sep. 2015, pp. 330–334. doi:10.18429/JACoW-IBIC2015-TUPB012